



Contents lists available at ScienceDirect

Journal of Orthopaedic Translation

journal homepage: www.journals.elsevier.com/journal-of-orthopaedic-translation

Puerarin specifically disrupts osteoclast activation via blocking integrin- β 3 Pyk2/Src/Cbl signaling pathway



Zuocheng Qiu^{a,b,1}, Ling Li^{a,1}, Yuying Huang^c, Keda Shi^a, Lizhong Zhang^a, Cuishan Huang^a, Jiechao Liang^a, Qingqiang Zeng^a, Jiali Wang^e, Xiangjiu He^c, Ling Qin^{a,d}, Xinluan Wang^{a,d,*}

^a Translational Medicine R&D Center, Institute of Biomedical and Health Engineering, Shenzhen Institutes of Advanced Technology, Chinese Academy of Sciences, Shenzhen 518057, China

^b Guangzhou Key Laboratory of Formula-Pattern of Traditional Chinese Medicine, Formula-Pattern Research Center, School of Traditional Chinese Medicine, Jinan University, Guangzhou, 510632, China

^c School of Pharmacy, Guangdong Pharmaceutical University, Guangzhou, 510006, China

^d Musculoskeletal Research Laboratory of Department of Orthopaedics & Traumatology, Innovative Orthopaedic Biomaterial and Drug Translational Research Laboratory of Li Ka Shing Institute of Health, The Chinese University of Hong Kong, Hong Kong SAR, China

^e School of Biomedical Engineering, Sun Yat-sen University, Guangzhou, 510275, China

ARTICLE INFO

Keywords:

Puerarin
F-actin ring
Integrin- β 3
Pyk2/Cbl/Src
Osteoclast activation

ABSTRACT

Objective: Given the limitations of current anti-resorption agents for postmenopausal osteoporosis, there is a need for alternatives without impairing coupling crosstalk between bone resorption and bone formation ie. osteoclastogenesis. Puerarin, a unique C-glycoside isoflavonoid, was found to be able to prevent bone loss by inhibiting bone resorption, but the underlying mechanism was controversial. In this study, we investigated the effects of puerarin on osteoclastic differentiation, activation and bone resorption and its underlying molecular mechanism *in vitro*, and then evaluated the effects of puerarin on bone metabolism using an ovariectomized (OVX) rat model. **Methods:** *In vitro*, the effect of puerarin on osteoclastic cytotoxicity, differentiation, apoptosis, activation and function were studied in raw 264.7 cells and mouse BMMs. Mechanistically, osteoclast-related makers were determined by RT-PCR, western blot, immunofluorescence, and kinase activity assay. *In vivo*, Micro-CT, histology, serum bone biomarker, and mechanical testing were used to evaluate the effects of puerarin on preventing osteoporosis.

Results: Puerarin significantly inhibited osteoclast activation and bone resorption, without affecting osteoclastogenesis or apoptosis. In terms of mechanism, the expressions of protein of integrin- β 3 and phosphorylations of Src, Pyk2 and Cbl were lower in puerarin group than those in the control group. Oral administration of puerarin prevented OVX-induced trabecular bone loss and significantly improved bone strength in rats. Moreover, puerarin significantly decreased trap positive osteoclast numbers and serum TRAP-5b, CTx1, without affecting bone formation rate.

Conclusions: Collectively, puerarin prevented the bone loss in OVX rat through suppression of osteoclast activation and bone resorption, by inhibiting integrin- β 3-Pyk2/Cbl/Src signaling pathway, without affecting osteoclasts formation or apoptosis.

Abbreviations: Atp6v0d2, ATPase H + Transporting V0 Subunit D2; BMD, Bone mineral density; BS, Bone surface; OVX, ovariectomized; BMMs, Bone marrow monocyte cells; BV/TV, Bone volume/tissue volume; c-Fos: Proto-oncogene C-Fos, Ct. Ar; Cortical area, CTx1; carboxyl-terminal telopeptides of type I collagen, CLCN7; Charge-coupled Cl-channel, CA II; Carbonic anhydrase II, Cs. Th; Cortical thickness, Conn. D; Connectivity density, CTSK; Cathepsin K, E₂; 17- β estradiol; Ec. Pm, Endocortical perimeter; ER, Estrogen receptor; M-CSF, Macrophage colony-stimulating factor; Src: Proto-oncogene tyrosine-protein kinase Src, Ma. Ar; Marrow area, MRM; Multiple reaction monitoring, MMP9; Matrix metalloproteinase-9, N. Oc; Number of trap positive osteoclasts, NFATc1; Nuclear factor of activated T cells 1, TRAP-5b; Tartrate-resistant acid phosphatase 5b, OC-STAMP; Osteoclast stimulatory transmembrane protein, OPG; Osteoprotegerin, Oc. S; Osteoclasts surface, P1NP; Amino-terminal propeptide of type I collagen, RANKL; Receptor activator of nuclear factor κ -B ligand, RLU; Luminescence, SD; Sprague–Dawley, rBMSC; rat bone marrow-derived mesenchymal stem cells. Tb. N, Trabecular number; Tb. Th, Trabecular thickness; Tb. Sp, Trabecular separation; TRAP, Tartrate resistant acid phosphatase; TRAF6, TNF-receptor-associated factor 6; TUNEL, Terminal deoxynucleotidyl transferase dUTP nick end labeling.

* Corresponding author. Translational Medicine R&D Center, Institute of Biomedical and Health Engineering, Shenzhen Institutes of Advanced Technology, Chinese Academy of Sciences, Shenzhen 518057, China.

E-mail address: xl.wang@siat.ac.cn (X. Wang).

¹ The authors contribute equally to this paper.

<https://doi.org/10.1016/j.jot.2022.01.003>

Received 29 September 2021; Received in revised form 24 January 2022; Accepted 24 January 2022

2214-031X/© 2022 The Authors. Published by Elsevier (Singapore) Pte Ltd on behalf of Chinese Speaking Orthopaedic Society. This is an open access article under the

CC BY-NC-ND license (<http://creativecommons.org/licenses/by-nc-nd/4.0/>).

Translational potential of this article: These results demonstrate the unique mechanism of puerarin on bone metabolism and provide a novel agent for prevention of postmenopausal osteoporosis.

1. Introduction

Osteoporosis is characterized by low bone mass and strength led to increased risk of fractures. It has become a serious issue to public health as the increasing aging people around the world. The imbalance of bone remodeling, i.e. osteoclastic bone resorption outraces osteoblastic bone formation was the pathogenesis of osteoporosis [1]. Thus, inhibition of bone resorption was considered as an effective way for the treatment of osteoporosis [1].

Several current available drugs are supposed to inhibit bone resorption, for instance, bisphosphonates are clinically used agents to suppress bone resorption [2], which induce the disruption of actin rings and apoptosis of osteoclast [3]. However, the decrease in bone resorption caused by bisphosphonates is soon accompanied by a decrease in bone formation. Unbalanced cooperation between osteoblasts and osteoclasts ultimately leads to poor bone quality, thereby limiting their efficacy [4]. Estrogen replacement therapy is a good alternative to inhibit osteoclastic bone resorption [5]. However, it also inhibits bone formation. Long term compliance with estrogen therapy is also limited by increasing concerns regarding its safety [6]. Thus, new classes of antiresorptive agents with a different mechanism of action from bisphosphonates and estrogen are still urgent to be developed.

One promising approach is the selective inhibition of bone resorption without interfering with the formation and survive of osteoclasts. The concept of cathepsin K (CatK) inhibitors brought breakthrough in this field [7]. Inhibitors of CatK showed impressive bone-preserving efficacies and keeping bone formation mostly unaffected in clinical trials. However, various side effects limited the approve of active site-directed inhibitors of CatK [7]. Then, a novel class of ectosteric antiresorptives were identified, and one of them was stem from Danshen, a traditional Chinese medicine (TCM) [4]. Increasing interest was risen on using natural products in medicinal and food herbs as alternatives in menopaual osteoporosis [8–10].

Puerarin (daidzein 8-C-glucoside) is a unique C-glycoside isoflavonoid isolated from the root of the *Puerariae lobate* (Willd) Ohwi, which is widely distributed in Southeast Asia and has been used as a food source, fodder, and medicine for thousands of years [11,12]. It has been extensively used in clinical practice for the treatment of cardiovascular diseases, diabetes, parkinson's disease, endometriosis, and cancer in China [12–14]. Our previous study found that puerarin promoted osteogenesis and inhibited adipogenesis *in vitro* [15]. It was reported puerarin prevented the OVX-induced bone loss by inhibiting osteoclastogenesis [16–19]. A recent study suggested puerarin suppressed osteoclastogenesis via NF- κ B signaling pathway [18,20]. However, others made distinct findings that puerarin did not affect the activation or expression of RANKL-induced osteoclastogenic signaling mediators and transcription factors, including CREB, PGC1 β , c-Fos and NFATc1 [21]. These inconsistent reports arouse our interest in continuous exploring the mechanism underlying the bone protective effect of puerarin.

In this study, we systematically explore the effects and underlying precise mechanism of puerarin on osteoclastogenesis, osteoclastic activation, and bone resorption *in vitro*. The ovariectomized rat model was used to mimic postmenopausal osteoporosis and investigate the effects of puerarin on regulating bone metabolism *in vivo*.

2. Materials and methods

2.1. Materials

Modified Eagle medium alpha (α -MEM), fetal bovine serum (FBS),

penicillin and streptomycin were purchased from Gibco (Gaithersburg, MD, USA). Phalloidin-iFluor 555 was purchased from Abcam (USA, #176756). Murine sRANKL and MCSF were the products of Peprotech (Rocky Hill, NJ, USA). Puerarin (standard, >99.31%, Lot.20150301) was purchased from Chengdu Herbpurify Corporation, LTD, (China) and E₂ (standard, >98%, Lot. #WXBC 2780V) was from Sigma–Aldrich (St. Louis, MO, USA). The following antibodies were used: rabbit monoclonal anti-integrin- β 3 (#13166, 1:1000), rabbit monoclonal anti-NFATc1 (#8032, 1:1000), rabbit polyclonal anti-c-Cbl (#2747, 1:500), rabbit polyclonal anti-Src (#2108, 1:1000), rabbit monoclonal anti-TRAF6 (#8028, 1:1000), rabbit monoclonal anti-NF- κ B p65 (#8242, 1:1000), rabbit monoclonal anti-p-NF- κ B-p65 (Ser536) (#3033S, 1:500), rabbit polyclonal anti-Paxilla (#2542, 1:1000), rabbit monoclonal anti-Gelsolin (#12953, 1:1000), rabbit polyclonal anti-Caspase-3 (#9662, 1:1000), and rabbit polyclonal anti-cleaved Caspase-3 (#9661,1:1000) were purchased from Cell Signaling Technology (Beverly, MA, USA); rabbit polyclonal anti-Pyk2 (BS-3357R, 1:500) and rabbit polyclonal anti-p-Pyk2 (Tyr402) (BS-3400R, 1:200) were provided from Bioss antibodies (Bioss, Beijing, China); rabbit monoclonal anti-p-Src (Tyr419) (sc-81521, 1:500), mouse monoclonal anti-p-Cbl (sc-377571) (sc-377571, 1:500) were purchased from Santa Cruz Biotechnology (Santa Cruz, CA, USA).

2.2. Cell culture and cytotoxicity assay

RAW 264.7 cells (ATCC, USA) were routinely cultured in modified Eagle medium alpha (α -MEM), supplemented with 10% fetal bovine serum (FBS), penicillin 100 U/mL and streptomycin 100 μ g/mL at 37 °C in a humidified atmosphere of 5% CO₂.

Primary bone marrow derived macrophages precursors were isolated from femur and tibia of 4-week-old to 6-week-old C57BL/6J mice (Beijing Huafukang Biotechnology Co., Ltd.,) according to a previous protocol [22]. The collected cells were used as bone marrow-derive macrophages (BMMs).

To determine the effect of puerarin on the cell viability, RAW264.7 cells and BMMs were seeded at 3000 cells/well or 8000 cells/well in 96-well plates, respectively. After 24 h of incubation, cells were treated with osteoclast differentiation medium (OCM, consist of α -MEM with 10% FBS, 100 ng/mL of RANKL, 30 ng/mL of M-CSF). After indicated time, CCK-8 solution was added, and cells were incubated at 37 °C for 2 h. Finally, absorbance was measured at 450 nm. Bone marrow mesenchymal stem cells (BMSCs) were isolated from SD rats according to a previous published protocol [23] and MC3T3-E1 cells were obtained from ATCC (USA), and the cells were seeded at 5000 cells/well in 96-well plates. After 24 h of incubation, cells were treated with different concentrations of puerarin. After indicated time, CCK-8 solution was added, and cells were incubated at 37 °C for 2 h. Finally, absorbance was measured at 450 nm.

2.3. Osteoclast differentiation and TRAP staining

RAW264.7 cells were seeded at 3000 cells/well in 96-well plates. After 24 h of incubation, cells were treated with different concentrations of puerarin (dissolved in DMSO) in OCM. After 4 days, TRAP staining was performed according to our previous method [24]. The number and spread area of multinucleated (number of nuclei \geq 3) osteoclasts were quantified under microscopy (Olympus IX71, USA).

2.4. Osteoclast apoptosis assay

RAW264.7 cells were seeded at 6000 cells/well in 48-well plates.

After 24 h of incubation, cells were treated with different concentrations of puerarin (dissolved in DMSO) in OCM for another 5 days. The apoptosis rate was assessed at a single cell level based on the labeling of DNA strand breaks [terminal deoxynucleotidyl transferase dUTP nick end labeling (TUNEL) technology] using the *In-Situ* cell death detection kit, Fluorescein (Roche Diagnostics GmbH, Mannheim, Germany) according to the manufacturer's protocol. TUNEL-positive cells were visualized under a fluorescence microscope (Leica, Germany). For quantification of apoptosis, cells were counted from 6 random selected views using image J software (Wayne Rasband, NIH, USA). The results were presented as a percentage of apoptotic cells over the total number of cells counted.

2.5. RT-PCR

RAW264.7 cells were seeded at 40,000 cells/well in 12-well plates. After 24 h, cells were treated with different concentrations of puerarin (dissolved in DMSO) in OCM for 2 or 4 days. Total RNA of RAW264.7 cells under different treatments was extracted using RNeasy kit (Qiagen, USA) according to the manufacturer's instructions. The reverse transcription was performed using PrimeScript™ RT Master Mix (TaKaRa, Japan). The primers sequences used in the assay were listed in [Supplementary Table 1](#). The 10 μ L of the final reaction solution contained 1 μ L of the diluted cDNA product, 5 μ L of 2 \times TB Green Premix Ex Taq II (TaKaRa, Japan), 0.5 μ L each of forward and reverse primers and 4 μ L nuclease free water. The amplification conditions and procedures were as the following: 50 °C for 2 min, 95 °C for 10 min, 40 cycles of 95 °C for 15 s, 60 °C for 1 min. The fluorescence signal was recorded by Roche Light Cycler 480 Detection System and then the signal was converted into numerical value. Relative gene expression was determined by employing the Comparative CT-method. The mRNA levels of all genes were normalized by β -actin as internal control. These analyses were performed in duplicates for each sample using cells from two different cultured wells, and each experiment was repeated with three times.

2.6. Western blot

RAW264.7 cells were seeded at 100,000 cells/well in 6-well plates. After 24 h, cells were treated with different concentrations of puerarin (dissolved in DMSO) for 4 days in OCM. Following that, cells were homogenized in RIPA lysis buffer containing 1% protease inhibitor cocktail (Roche, USA) and 1% phosphate inhibitor cocktail (Roche, USA). Total protein of cell lysates was quantified with BCA protein assay kit (Beyotime Biotechnology, China). PageRuler Prestained Protein Ladder (00758179, Thermo Fisher, USA) was used as loading marker. Equal amounts of protein (40 μ g) in each sample were separated by 10% SDS-polyacrylamide gel electrophoresis (SDS-PAGE) and transferred to polyvinylidene fluoride (PVDF) membranes (Millipore) at 300 mA for 70 min, following blocked with 5% milk in TBST and probed with primary antibodies. The blots were subsequently probed with HRP AffiniPure Goat Anti-rabbit or Anti-mouse IgG (H + L) (1:2000 dilution, EarthOx, USA) as secondary antibodies. Band signals were detected with Millipore Immobilon Western chemiluminescent horseradish peroxidase substrate (Millipore Corporation, Billerica, MA, USA) and quantitated using Image J analysis software (Wayne Rasband, NIH, USA). Relative protein expressions were normalized to the GAPDH or β -actin expression level.

2.7. Immunofluorescence staining for F-actin and integrin β 3 of osteoclasts

RAW264.7 cells and BMMs were seeded at 3000 and 8000 cells/well onto the Corning® Osteo Assay Surface 96-well plates (Corning Incorporated Life Science, NY, USA), respectively. RAW264.7 cells were cultured in OCM with the treatment of puerarin for 4 days, while BMMs were treated for 10 days. After the treatment, RAW264.7 cells and BMMs were rinsed with PBS for 3 times and fixation in 4% formaldehyde for 30 min at 4 °C. Then, cells were permeabilized for 10 min in 0.1% X-100 in

PBS. After a brief washing in PBS, cells were blocked with 5% bovine serum albumin for 1 h and then incubated with integrin β 3 antibody (1:200, CST, USA) overnight. Cells were then incubated with Alexa Fluor 488-labeled Goat Anti-Rabbit IgG(H + L) (1:250, Beyotime, A0423, China) for 2 h. Following that, cells were incubated with Phalloidin-iFluor 555 (Abcam, USA) for 2 h to label the F-actin ring according to a previously described method [25]. After treatment with acting ring staining, cells were washed three times with PBS followed by staining nuclei with DAPI (Beyotime Biotechnology, China) for 5 min, cells were visualized using fluorescence microscope (Leica, DMI8) or confocal microscope (Nikon, A1R). Six wells were selected in each group to calculate the number of the F-actin ring cells using Image-Pro plus 6.0 software (Media Cybernetics, Silver Spring, MD, USA).

2.8. Resorption pit assay

RAW264.7 cells seeded at 3000 cells/well onto the Corning® Osteo Assay Surface (Ca-P) 96-well plate (Corning, NY, USA). After 24 h of incubation, cells were treated within OCM. The drug treatment medium was replaced every 2 days. At day 7, The cells were removed by treating each well with 5% sodium hypochlorite for 5 min and wash with water and dry. The wells were imaged with microscopy (Olympus IX71, USA) to identify resorbed pits. The area of bone resorbed pits was quantified using Image-Pro Plus 6.0 software (Media Cybernetics, Silver Spring, MD, USA). BMMs were seed at 8000 cells per well at sterile bovine cortical bone slices (diameter: 6 mm; thickness: 0.1 mm) coated in a 96-well plate, after 24 h, cells were replaced with RANKL (100 ng/mL, Peprotech) and M-CSF (30 ng/mL) in the absent or present of puerarin (1000 mM, dissolved in DMSO) for 10 days. Cells attached to bone slices were scratched by cotton swab. The slices were dried before a thin gold-palladium film was sputtered to impart conductivity to samples, the resorbed pits formed on the slices were determined by scanning electron microscopy at 5 kV (ZEISS, SUPRA 55 SAPPHIRE).

2.9. Src kinase activity assay

The Src kinase activity was measured with or without puerarin (dissolved in DMSO) by using ADP-Glo™ kinase luminescent assay combined with Src Kinase Enzyme System according to the manufacturer's protocol. Saracatinib (MedChemExpress, hy-10234, USA) was used as a positive Src kinase inhibitor. Relative Luminescence Unit (RLU) was recorded with a microplate reader (BioTek Synergy H1, USA) upon incubation with Kinase Detection Reagent. The IC₅₀ of Src kinase activity was calculated by fitting the experimental data to Prism 8.0.

2.10. Animal studies

Forty-five 6-month-old female Sprague–Dawley (SD) rats (body weight 230.6 \pm 10.3 g) for a long-term study (12 weeks) and thirty-six 6-month-old female SD rats (body weight 269.84 \pm 11.76 g) for a short-term study (5 weeks) were provided and maintained in a common facility at School of Pharmacy, Guangdong Pharmaceutical University (Guangzhou, China). These animals were housed in a temperature-controlled room (25 °C) at 75% humidity under a 12/12h reversed day/night cycle and received food and water. They were fed maintenance diet (Diet No: 11002900029794, Beijing Ke Ao Xie Li Feed Co., Ltd, Beijing, China). The animal experimental followed in compliance with the guiding principles in the Guide for the Care and Use of Laboratory Animals: Eighth Edition, ISBN-10: 0-309-15396-4 and the protocol was approved by the Research Ethics Committee of Shenzhen Institutes of Advanced Technology.

The rats were divided into different groups randomized according to average weight by using the random function in excels. In the long-term study, the rats were either sham-operated (Sham, n = 9) or ovariectomized for establishing the estrogen depletion animal model to mimic the clinical condition of menopausal women based on our established

protocol (OVX, $n = 36$). The OVX rats were randomly assigned into the following four groups: OVX group, estradiol treatment group (E_2 , 1 mg/kg/day, once daily administration (qd), intragastric administration (i.g.)), low dose puerarin (L-Puerarin, 50 mg/kg/day, qd, i.g.), and high dose puerarin (H-Puerarin, 150 mg/kg/day, qd, i.g.). In the short-term study, the rats were either sham-operated (Sham, $n = 9$) or ovariectomized (OVX, $n = 9$ for each group). The OVX rats were randomly assigned into the following three groups: OVX group, estradiol treatment group (E_2 , 1 mg/kg/day, qd, i.g.), and high dose puerarin (H-Puerarin, twice daily administration of 75 mg/kg (bid), i.g.). The rats were induced with 3.5% isoflurane and maintained anesthesia with 2.5% isoflurane. Bilateral ovariectomy were performed in all groups except the sham-operated group. One dose of Ketoprofen Gel (Menarini Manufacturing Logistics and Services, Firenze, Italy) was applied to surgical wounds for analgesic coverage after surgery. Restored for three days after Sham or OVX operation, the treatment started. In the long-term study, both the Sham and OVX rats were treated with 0.5% CMC-Na, the vehicle was used to suspend puerarin and E_2 . In the short-term study, 0.9% normal saline was used to dissolve the puerarin (powder for injection, Lot.170403, Zhe Jiang Zhen Yuan Pharmaceutical Co., Ltd., Zhejiang, China) and 0.5% CMC-Na was used to dissolve E_2 . Both Sham and OVX rats were treated with 0.5% CMC-Na, and 0.9% normal saline simultaneously. All rats were injected subcutaneously with 1% calcein green (Lot: #MKCF4867, Sigma) in a time sequence of 13, 12 and 3, 2 days before euthanasia for studying bone mineral apposition. All rats were sacrificed using pentobarbital sodium (intraperitoneally, 120 mg/kg body weight) at the end of treatment. Blood sample was collected from heart for serum isolation by centrifugation. Uterus was obtained and weighed and then stored in 10% formalin solution for histomorphology. The left femur was kept in 50:50 saline-ethanol solution for biomechanical testing. The left tibia was preserved in 10% formalin solution and transferred into 70% ethanol after 48 h for measurement of trabecular micro-architecture by micro computed tomography (Micro CT) and histomorphology.

2.11. Regions of interests for in vivo evaluations

In Micro-CT analysis, 150 continuous slices beginning at 1.0 mm from the most distal aspect of the growth plate extending distally along the proximal tibia diaphysis were selected for analysis. For tibia diaphysis, 150 continuous slices beginning from connection of tibia and fibula extending distally along the proximal tibia diaphysis were selected for analysis. A material test machine (H25KS; Hounsfield Test Equipment Ltd. UK) with a 250 N load cell was used for three-point-bending test of the left femur diaphysis. Bone histomorphometric parameters were measured from at least 1 mm from the growth plate to 4 mm, excluding the primary spongiosa using the Image-Pro Plus (Media Cybernetics, Silver Spring, MD, USA) [26].

2.12. Micro-computed tomography (micro CT) analysis

Proximal tibias and tibia diaphysis from each group were subjected to be scanned by Micro CT system (SCANCO Medical 100, SCANCO Medical AG, Zurich, Switzerland) followed with a resolution of 18 μm , 70 kV energy, 200 A intensity, and 150 ms integration time. After regions of interests of proximal tibia and tibia diaphysis were selected as above. All the trabecular bone and cortical bone from each selected slice were segmented for 3D reconstruction to calculate bone mineral density (BMD, %). The threshold of trabecular bone was set from 52 to 255 and cortical bone was set from 50 to 255. Bone volume/tissue volume (BV/TV), trabecular number (Tb. N), trabecular thickness (Tb. Th), and trabecular separation (Tb. Sp) were calculated for trabecular bone. Cortical area fraction (Ct. Ar/Tt. Ar), cortical area (Ct. Ar), Marrow area (Ma. Ar), endocortical perimeter (Ec. Pm) and cortical thickness (Cs. Th) were calculated for cortical bone [27,28].

2.13. Mechanical testing

Left femurs from each group were kept with 0.9% saline solution in -80 centigrade for mechanical testing. A material test machine (H25KS; Hounsfield Test Equipment Ltd. UK) with a 250 N load cell was used for three-point-bending test. The left femur diaphysis was positioned horizontally with the anterior surface upwards, centered on the supports with 20 mm apart. A displacement rate of 5 mm/min was selected for applying the loading vertically to mid-shaft with anterior surface upward using our established protocol [29]. Ultimate load (N) and displacement (mm) were recorded until material failure for statistical comparison. Energy to failure was calculated.

2.14. Histological and histomorphometry analysis

2.14.1. Bone Von Kossa staining and fluorescence labeling

Proximal tibia metaphysis of nine samples from each group were isolated and dehydrated in graded concentrations of ethanol, defatted in acetone, and embedded without decalcification in modified methyl methacrylate. Coronal sections for trabecular bone were prepared at a thickness of 5 μm and 8 μm with Tungsten Steel by Manual Rotary Microtome (RM2235, Leica Biosystems, Inc., Buffalo Grove, USA). Plastic of 5 μm slices in each group ($n = 9$) were subjected to Von Kossa staining for static histomorphometric analysis. Plastic of 8 μm slices in each group ($n = 9$) were removed and sealed by neutral resin for histological images digitalized with a microscopic imaging system (Leica DMI8, Leica Microsystems, Weztlar, Germany) under the fluorescence mode for dynamic histomorphometric analysis. Static parameters such as total tissue area (T. Ar), bone area (B. Ar), bone perimeter (B.Pm) were obtained in white light slice. The bone volume (BV/TV), trabecular number (Tb.N), trabecular separation (Tb.Sp) and trabecular width (Tb.Wi) were calculated as described by Dempster et al. [26]. Dynamic parameters such as single-labeled perimeter (sL. Pm), double-labeled perimeter (dL. Pm), interlabeled width (Ir.L.Wi) were measured in fluorescence slice. The Mineralizing surface (MS/BS), mineral apposition rate (MAR) and bone formation rate fraction with bone surface (BFR/BS) were calculated as described by Dempster [26].

2.15. Bone tartrate-resistant acid phosphatase (TRAP) staining

Left tibia of nine samples from each group were decalcified with 0.5 mol/L ethylene diamine tetra acetic acid (EDTA) solution (pH = 7.4) in 37 °C shaker, renewed EDTA solution everyday till decalcified completely. And then embedded with paraffin. 5 μm -thick paraffin coronal section was cut by Manual Rotary Microtome (RM2235, Leica Biosystems, Inc., Buffalo Grove, USA). Tartrate-resistant acid phosphatase (TRAP) Staining were stained with acid phosphatase leukocyte (TRAP) Kit (Sigma-Aldrich, USA) according to manufacturer's instruction for counting osteoclast. An optical microscope (Leica DMI8, Leica Microsystems, Weztlar, Germany) was used for observation and acquisition. Osteoclasts were the cells with multiple nuclei and stained purple. The number of purple osteoclasts (N.TRAP⁺-Oc), TRAP-positive osteoclasts surface (TRAP⁺-Oc.S) surrounding the trabeculae and trabecular bone surface (BS) from the area of 1 mm under the growth plate excluding the primary spongiosa to 4 mm along bone diaphysis was measured using the Image-Pro Plus (Media Cybernetics, Silver Spring, MD, USA). The TRAP-positive osteoclast index was calculated as the number of osteoclasts divided by the trabecular bone perimeter (N.TRAP⁺-Oc/BS) and TRAP-positive osteoclast surface divided by the trabecular bone surface (TRAP⁺-Oc.S/BS).

2.16. Uterine H&E staining

Middle aspect of uterus relative to the cervix of nine samples from each group were dehydrated in grade concentrations of ethanol, removed ethanol in dimethylbenzene and embedded in paraffin. 5 μm -thick

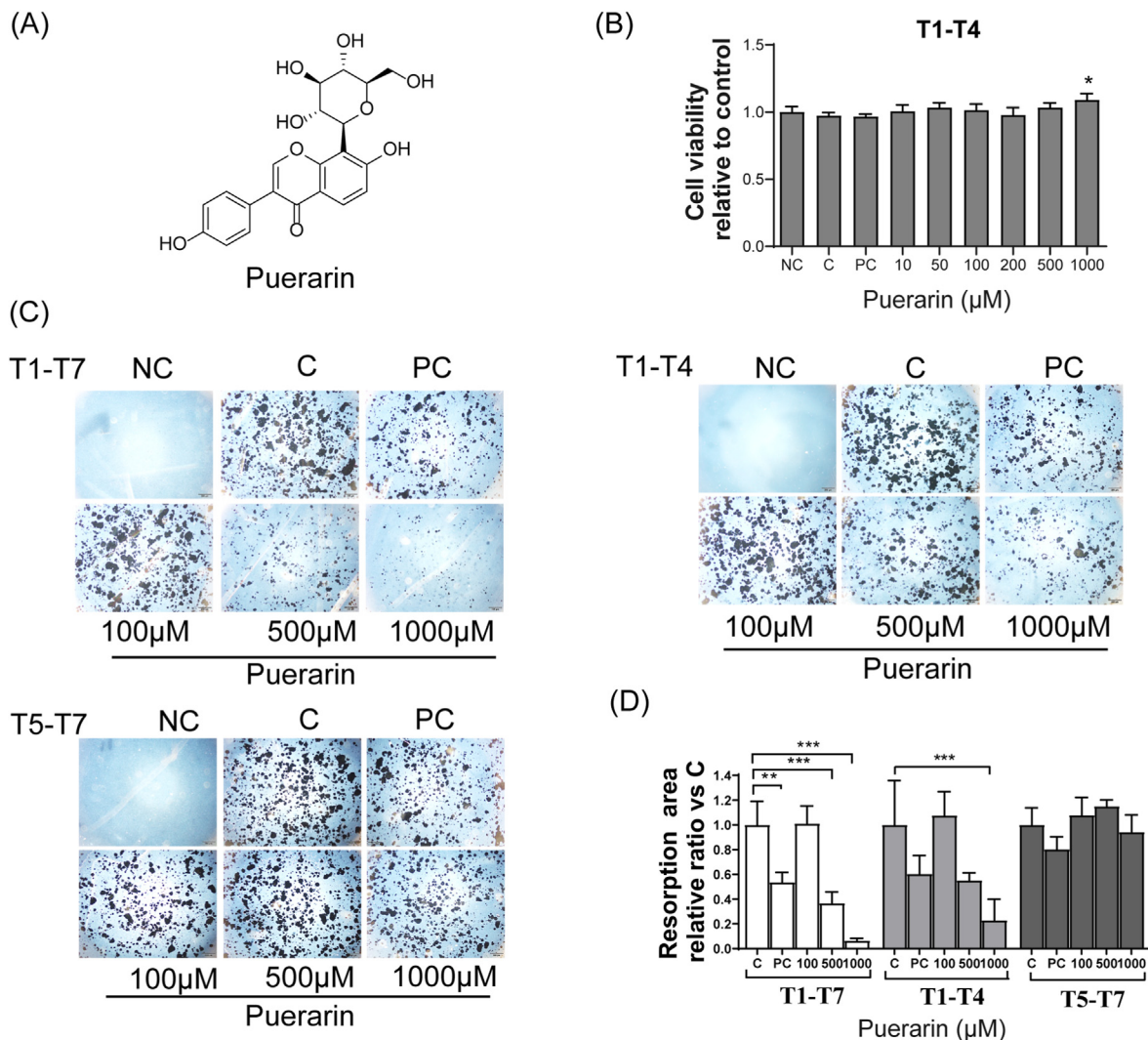


Fig. 1. Puerarin inhibits bone resorption during osteoclast maturation (A) The chemical structure of puerarin (B) The viability of RAW264.7 cells were determined at day 4 after treatment with puerarin under osteoclast differentiation medium (OCM) for day 1 to day 4 ($n = 6$) (C) Representative images of resorbed pits determined at day 7 after RAW264.7 cell under OCM with treatment of puerarin from day 1 to day 7 (T1-T7), day 1 to day 4 (T1-T4), day 5-day 7 (T5-T7), respectively. Scale bar is 100 μm (D) Resorbed pits formed by osteoclast induced from RAW264.7 cell per well was quantified and normalized relative to control ($n = 5$). NC: Negative control (0.1% DMSO), cells without drug treatment in the absent of OCM; C: Control (0.1% DMSO), cells without drug treatment; PC: Positive control, cells treated with 17- β estradiol (E_2 , 0.01 μM). The groups of C, PC, and different concentration of puerarin were induced by OCM. Data expressed are means \pm SD; * $P < 0.05$, significantly different from the control group.

paraffin transections were cut by Manual Rotary Microtome (RM2235, Leica Biosystems, Inc., Buffalo Grove, USA). The whole endometrial cell height was measured on 5 μm -thick hematoxylin-eosin-stained sections using the Image-Pro Plus (Media Cybernetics, Silver Spring, MD, USA).

2.17. ELISA assay for bone metabolism biomarker

Serum sample size for biomarkers determination was six in each group because hemolysis or insufficient acquisition appeared in several blood samples of each group. Bone formation markers in serum, including amino-terminal propeptide of type I collagen (P1NP) and bone resorption marker, carboxyl-terminal telopeptides of type I collagen (CTx1) were assayed using ELISA kits (PAA957Ra01 for P1NP, CEA665Ra for CTx1, Cloud clone Corp., Wuhan, China) and tartrate-resistant acid phosphatase (TRAP) were performed with ELISA kits (SB-TR201A, IDS Ltd., Boldon, UK) according to the manufacturer's protocol. Five calibrators for P1NP and CTx1, meanwhile, four calibrators for TRAP were measured for the standard curve according to manufacturer's

manual. All the results were normalized against bone mass values in Micro CT [30].

2.18. UPLC-MS/MS for E_2

Serum from animal samples were also used to determinate the content of estrogen by UPLC-MS/MS system. The quantitative analysis was performed on a UPLC-MS/MS system consisting of ACQUITY™ UPLC System (Waters Corp., Milford, USA) coupled to a Xevo TQ-XS mass spectrometer (Waters Corp., Milford, USA). The sample preparation method, derivatization and determination were consistent with that reported in the literature [31,32].

2.19. Data and statistical analysis

Studies were designed to generate groups of $n \geq 3$. The n value for each experiment was show in the figure legend. All data were expressed as mean \pm standard deviation of the mean (SD) based on at least three

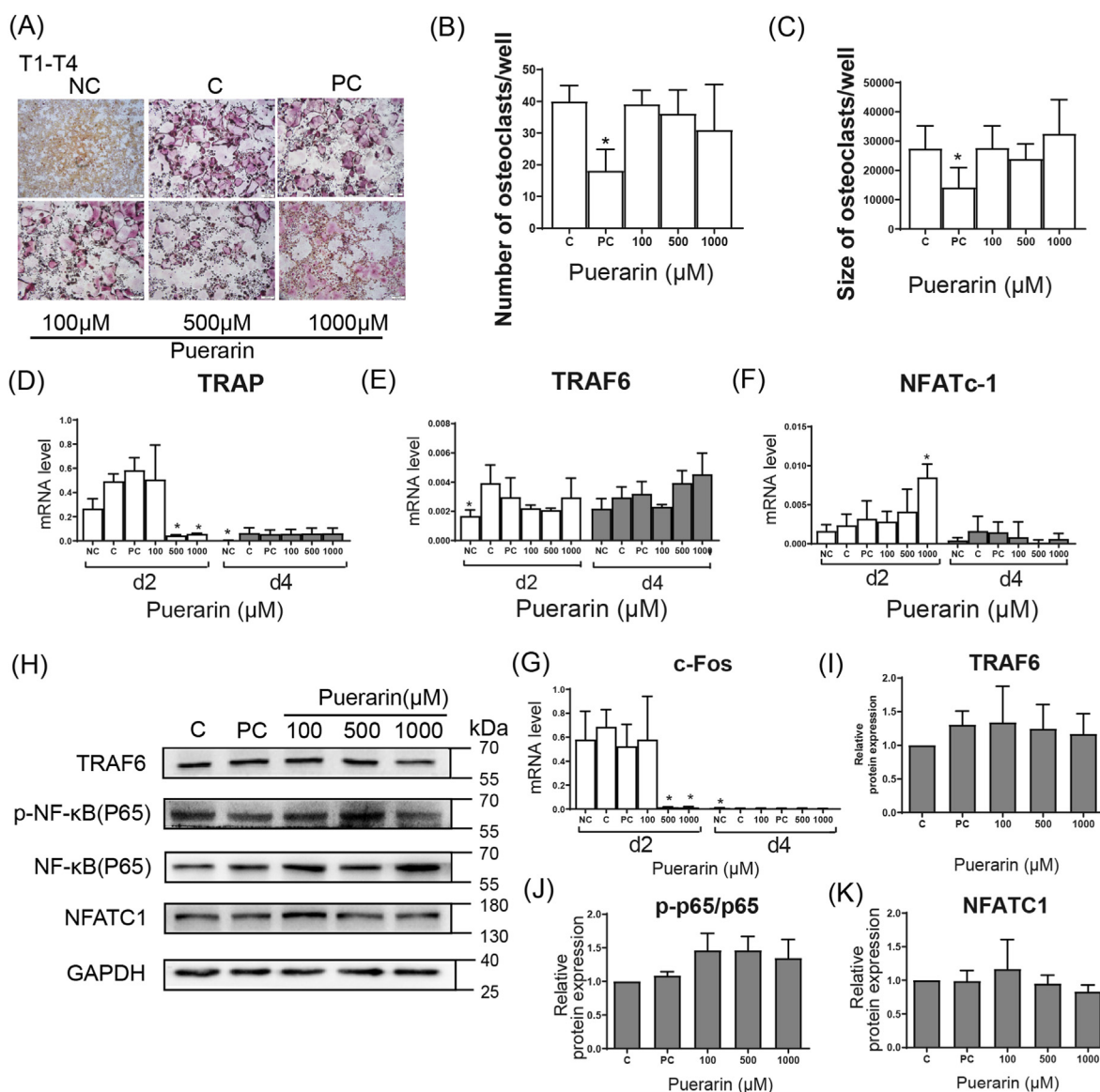


Fig. 2. Puerarin does not affect osteoclast differentiation (A) Representative pictures of TRAP staining at day 4 after RAW264.7 cells cultured under OCM with the treatment of drugs at day 1 to day 4 (T1-T4). Scale bar is 200 μm (B) Quantitative of number of osteoclasts (TRAP positive and multi-nucleated cells (MNCs), more than 3 nuclei) (n = 5) (C) Size of osteoclast per well was calculated by total area of MNCs/number of MNCs (n = 5) (D–G) mRNA expression of osteoclast differentiation related genes under OCM with the treatment of puerarin for 2 or 4 days (n = 5) (H) Representative blots of osteoclast differentiation related proteins under OCM with the treatment of puerarin for 4 days (I–K) Band intensities were semi-quantified and normalized relative to GAPDH (n = 5). NC: Negative control, cells treated with vehicle (0.1% DMSO) in the absent of OCM; The groups of C, PC, and different concentration of puerarin were all induced by OCM. C: Control, cells treated with vehicle (0.1% DMSO); PC: Positive control, cells treated with 17-β estradiol (E₂, 0.01 μM), Puerarin (100–1000 μM): cells treated with different concentrations of puerarin (dissolved in DMSO). Data expressed are means ± SD; *P < 0.05, ***P < 0.001, significantly different from the control group.

independent experiments. The significance of differences between groups was analyzed by one-way analysis of variance (ANOVA) followed by Tukey *post hoc* test. The PRISM software version 8.0 (GraphPad, San Diego, CA, USA) was used. P < 0.05 was considered as significant.

3. Results

3.1. Puerarin attenuated bone resorption without impairing cell viability of osteoclasts

The chemical structure of puerarin was shown in Fig. 1A. After 4 days treatment, no toxic effects were observed in RAW264.7 cells at various concentrations of puerarin as indicated, and even a significant promotion effect on cell viability was observed at 1000 μM (Fig. 1B). Also, no toxic

effects were visualized on other bone cells including mouse BMMs, rat BMSC and MC3T3-E1 cells under the treatment of puerarin for 2 days (Fig. S1). The area of resorbed pits formed by osteoclasts of RANKL-induced RAW264.7 cells was not affected by various concentrations of puerarin below 50 μM (Fig. S2H), but significantly decreased by puerarin treated in the early stage (T1-T4) (1000 μM puerarin vs. control) and the full stage (T1-T7) (500 and 1000 μM puerarin vs. control), but not the late stage (T5-T7) (Fig. 1C and D). Moreover, mRNA expressions of cathepsin K (CTSK) and matrix metalloproteinase-9 (MMP9) were not significantly affected by puerarin treatment (Fig. S3A and S3B), which indicated that puerarin did not directly inhibit bone resorption. The above results suggesting that puerarin inhibits the bone resorption activity at the osteoclast activation stage (T1-T4) rather than at the function stage (T5-T7).

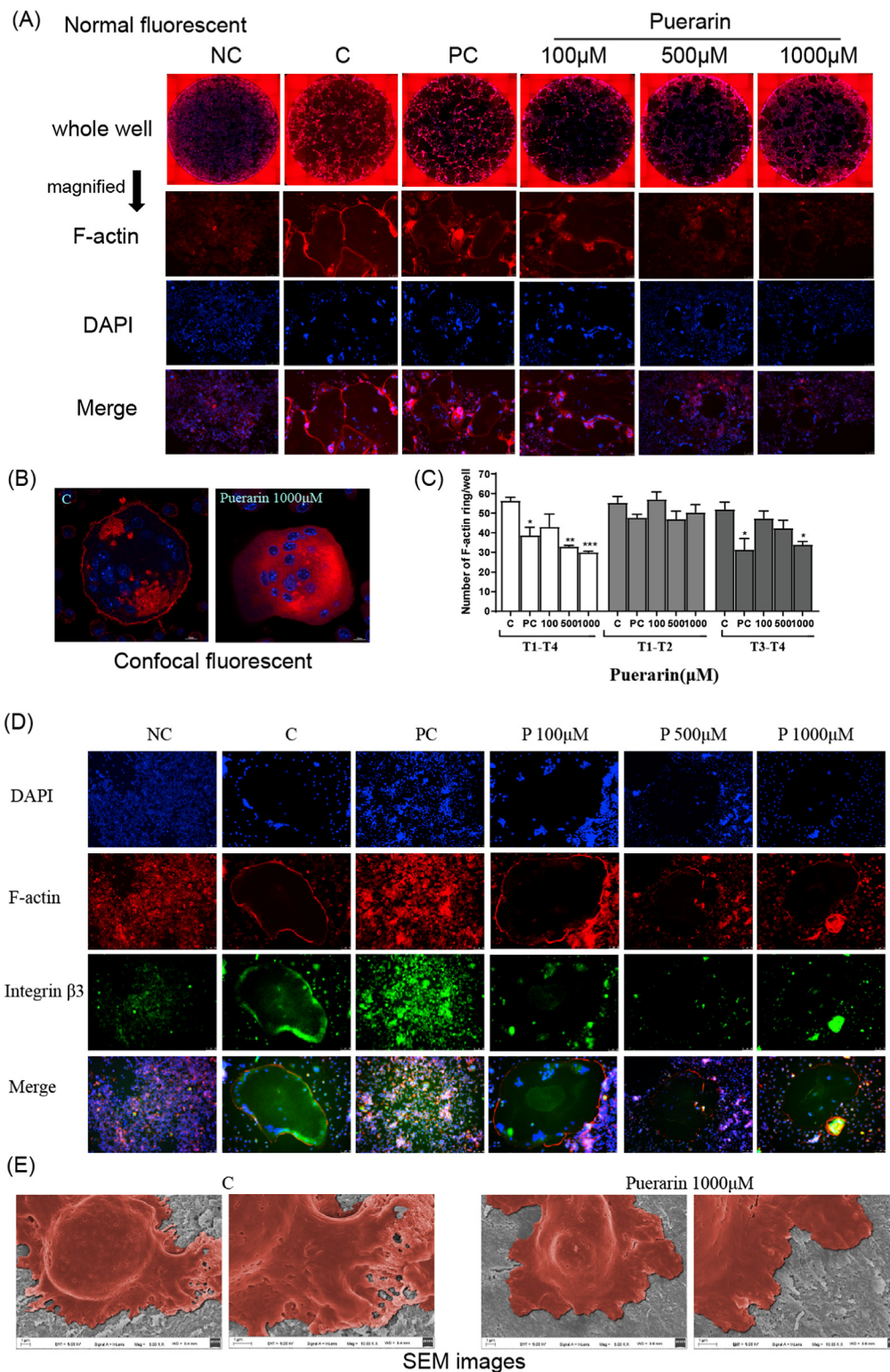


Fig. 3. Puerarin disturbs F-actin ring formation of osteoclast (A) Representative fluorescence images of F-actin ring formation in osteoclasts from RAW264.7 cells under OCM for 4 days. Cells were fixed in 4% paraformaldehyde for 15 min and stained for phalloidin (red) and counterstained with DAPI (blue). Scale bar is 100 μm (B) Representative images of F-actin ring in osteoclast snapped by confocal immunofluorescence microscopy; F-actin (red), nuclei(blue), Scale bar is 10 μm (C) Number of F-actin ring in osteoclast of RAW264.7 cells under OCM for 4 days with treatment of puerarin for day 1 to day 4 (T1-T4), day 1 to day 2 (T1-T2), day 3 to day 4 (T3-T4) were quantified (n = 5) (D) Representative images of F-actin and integrin β3 co-stained osteoclasts, the osteoclasts were induced from BMMs for 10 days under drug treatment; Cells were double stained for integrin-β3 (green) , phalloidin (red) and counterstained with DAPI (blue). Scale bar is 100 μm (E) Structure of osteoclast induced by BMMs attached on bone slice was snapped by SEM at day 10 (n = 3). Scale bar is 1 μm; NC: Negative control, cells treated with vehicle (0.1% DMSO) in the absent of OCM; The groups of C, PC, and different concentration of puerarin were induced by OCM. C: Control, cells treated with vehicle (0.1% DMSO); PC: Positive control, cells treated with 17-β estradiol (E₂, 0.01 μM), Puerarin (100–1000 μM); cells treated with different concentrations of puerarin (dissolved in DMSO). Data expressed are means ± SD; *P < 0.05, significantly different from the control group.

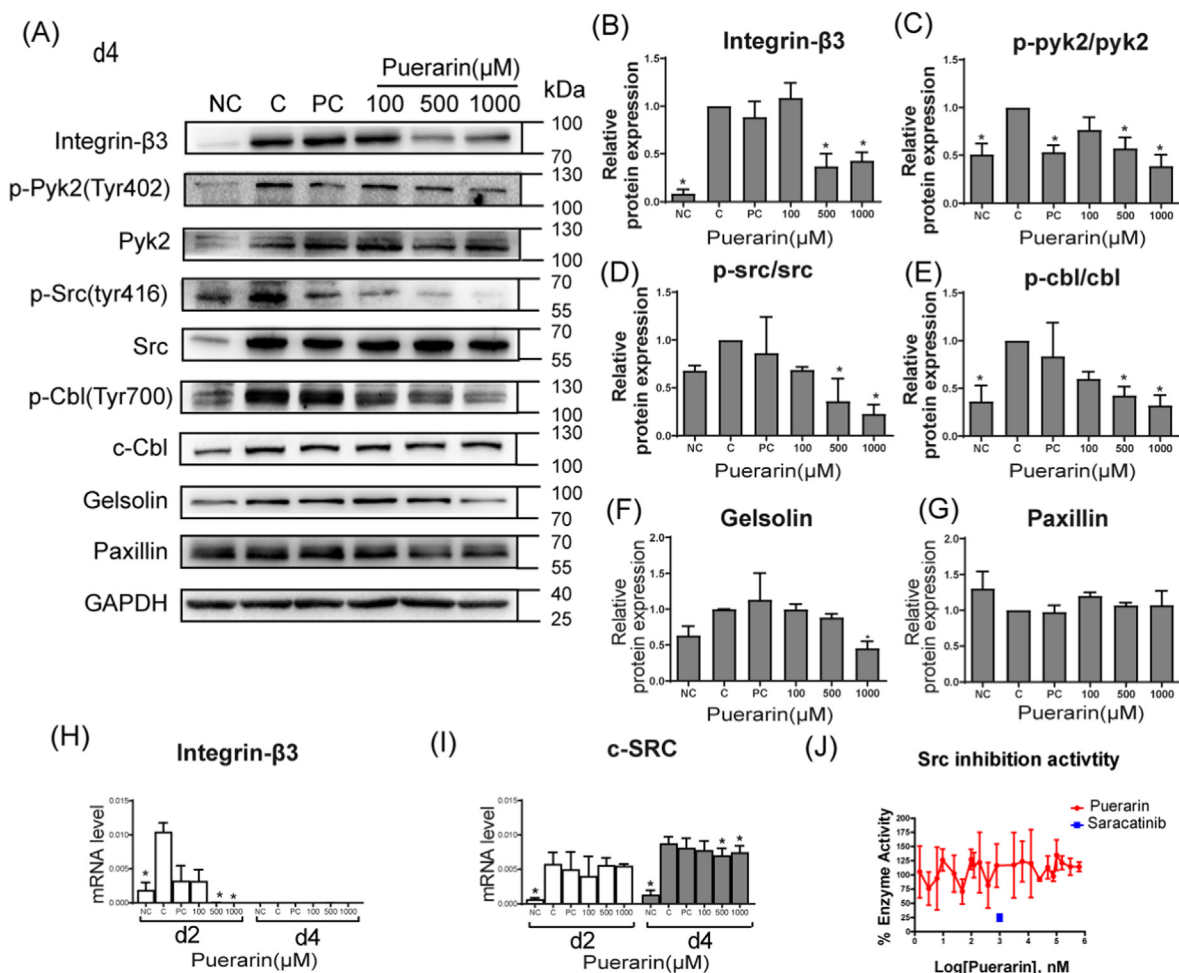


Fig. 4. Puerarin disturbs F-actin ring formation via depressing Integrin-β3-mediated Pyk2-Src-Cbl pathway (A) Representative blots of Pyk2-Src-Cbl signaling pathway related proteins were determined at day 4 under the treatment of puerarin for day 1 to day 4 in OCM (B–G) Band intensities were quantified and normalized relative to GAPDH (n = 5) (H–I) mRNA expression of Integrin-β3 and c-Src related to β-actin under OCM with the treatment of puerarin for 2 or 4 days (n = 5) (J) Inhibition curves of puerarin on Src kinase activity. Saracatinib (1000 nM) was a positive Src kinase inhibitor (n = 5); NC: Negative control, cells treated with vehicle (0.1% DMSO) in the absent of OCM; The groups of C, PC, and different concentration of puerarin were induced by OCM. C: Control, cells treated with vehicle (0.1% DMSO); PC: Positive control, cells treated with 17-β estradiol (E₂, 0.01 μM), Puerarin (100–1000 μM): cells treated with different concentrations of puerarin (dissolved in DMSO). Data expressed are means ± SD; *P < 0.05, significantly different from the control group.

3.2. Puerarin disrupted osteoclast activation but did not affect early stage of osteoclastogenesis

Osteoclast activation mainly includes two stages: osteoclastogenesis and osteoclast activation, the effect of puerarin on the two stages were further determined by TRAP-stained, RT-PCR, and western blot. As indicated in Fig. 2A–C, the number of TRAP-positive multinucleated osteoclasts (more than 3 nuclei) was not significantly diminished by puerarin (10–1000 μM) (Fig. 2A and B, Fig. S2A–D). However, we observed in Fig. 2A that many multiple-nucleated osteoclasts in the puerarin groups were TRAP low-staining osteoclast. Normalization of area to the number of multinucleated osteoclasts suggested that the size of osteoclast was not significantly affected by puerarin (Fig. 2C). Moreover, we observed in the light microscope that single nucleated monocytes fused to multi-nucleated osteoclasts were not influenced by various concentrations of puerarin during RANKL-induced for 4 days (Fig. S2A). RT-PCR data showed that OC-STAMP, which determined cell fusion and size of osteoclast, was not significantly affected by puerarin (Fig. S3C). Therefore, puerarin may not affect the early stage of osteoclastogenesis and cell fusion. However, the color of most TRAP staining positive osteoclasts was attenuated by puerarin at concentrations of 500 and 1000 μM (Fig. 2A), which is consistent with the result that TRAP gene

expression was also strongly down regulated by puerarin at concentrations of 500 and 1000 μM at day 2, but not day 4 after induction (Fig. 2D). In addition, TRAF6 was not influenced at day 2 and 4 (Fig. 2E), and NFATc1 was even up regulated by puerarin at the concentration of 1000 μM at day 2 (Fig. 2F). In contrast, c-Fos was significantly down-regulated by puerarin at concentrations of 500, 1000 μM at day 2 after induction (Fig. 2G). For the expression of osteoclast mature-associated genes, CAII (Fig. S3D) and TCIRG (Fig. S3E) were down-regulated at day 2 after induction, Atp6v0d2 (Fig. S3F) and CLCN7 (Fig. S3G) were unaffected at day 4 after induction. For the western blot analysis on the expression of osteoclastogenesis related proteins: TRAF6 (Fig. 2I and H), the ratio of phosphorylation of NF-κB p65/p65 (Fig. 2J and H), and NFATc1 (Fig. 2K and H) were all not altered by puerarin at day 4, and the same result was also obtained at day 2.

3.3. Puerarin disrupted F-actin ring formation via down-regulating integrin-β3 Pyk2/Src/Cbl signaling pathway

As the phalloidin-Alexa Fluor 555 staining of osteoclast induced from RAW264.7 cells shown in Fig. 3A–B, and Fig. S2E–F, characteristic F-actin rings formed well in the RANKL-induced control group and puerarin of concentration below 100 μM, but the structure of F-actin ring was

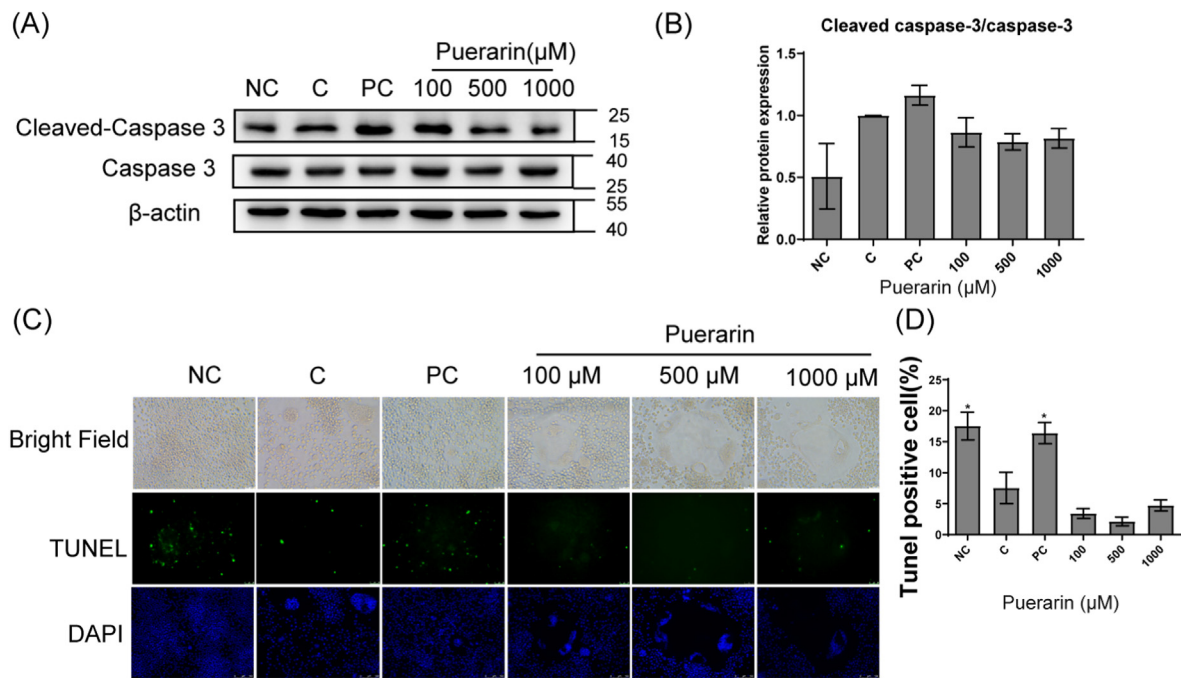


Fig. 5. Puerarin does not affect osteoclast apoptosis. RAW264.7 cells were cultured under OCM with different treatments for 5 days (A) Representative blots of cell apoptosis related proteins (B) The ratio of cleaved caspase-3/caspase-3, Band intensities were quantified and normalized relative to β -actin (n = 5) (C) Representative TUNEL staining of apoptosis osteoclasts; Scaled bar: 50 μ m (D) The percentage of apoptosis cells (TUNEL positive cells) in total cells (%) (n = 5); NC: Negative control, cells treated with vehicle (0.1% DMSO) in the absent of OCM; The groups of C, PC, and different concentration of puerarin were induced by OCM. C: Control, cells treated with vehicle (0.1% DMSO); PC: Positive control, cells treated with 17- β estradiol (E_2 , 0.01 μ M), Puerarin (100–1000 μ M): cells treated with different concentrations of puerarin (dissolved in DMSO). Data expressed are means \pm SD; *P < 0.05, significantly different from the control group.

disrupted by puerarin in a dose-dependent manner (500–1000 μ M). In contrast, 17- β estradiol (E_2 , 0.01 μ M) only slightly disrupted it. The number of F-actin formation was further quantified, as indicated in Fig. 3C, puerarin (500–1000 μ M) diminished the number of F-actin rings in osteoclast at the stage of T3–T4 and the stage of T1–T4, but not at the very early stage (T1–T2).

The disruption of F-actin ring by puerarin also appeared in RANKL-induced BMMs (Fig. 3D). To further demonstrate the effect of puerarin on actin ring organization, osteoclast was co-immunofluorescence staining with integrin β_3 , the actin-binding protein. It indicated that the fluorescence intensity of integrin β_3 (green) co-localized with F-actin core of podosome was significantly attenuated by puerarin in a dose dependently manner (Fig. 3D). In order to clearly visualize the structure of osteoclast induced by BMMs, scanning electron microscopy was applied. As showed in Fig. 3E, the mature osteoclasts in the control group with classic morphological features attaching well in the bone slices, whereas the morphology of osteoclast was abnormal after treated with puerarin (1000 μ M).

Integrin- β_3 /Pyk2/Src/Cbl signaling pathway regulates F-actin formation in osteoclasts induced by RANKL. As the blots shown in Fig. 4A, the expression of integrin- β_3 was significantly down-regulated by puerarin at the concentration of 500 and 1000 μ M (Fig. 4B), which corresponding with the result of immunofluorescence staining (Fig. 3D). Following that, the relative ratio of p-Pyk2/Pyk2 (Fig. 4C), p-Src/Src (Fig. 4D), p-Cbl/Cbl (Fig. 4E), were suppressed by puerarin in a dose-dependent manner. In contrast, the total protein of Pyk2, Src, Cbl seems not to have been affected by puerarin (Fig S1D–F). Moreover, the F-actin enriched proteins that organized F-actin ring: gelsolin, but not paxillin, was suppressed by 1000 μ M of puerarin (Fig. 4F and G). Consistent with protein expression, gene expression of integrin- β_3 was also down-regulated by puerarin (500, 1000 μ M) at day 2 after induction (Fig. 4H), while at day 4, the gene expression was too low to detect. The gene expression of Src (Fig. 4I) was not inhibited by puerarin at day 2, while only slightly inhibit by puerarin (500, 1000 μ M) at day 4, which

was consistent with its protein expression (Fig. 4A). In addition, kinase activity of Src (Fig. 4J) was also not affected by puerarin.

3.4. Puerarin did not affect osteoclast apoptosis

The apoptosis of osteoclasts was also detected. The number of TRAP-positive multinucleated cells (more than 3 nuclei) were defined as osteoclast. The ratio of cleaved caspase-3/caspase-3 was up-regulated by E_2 (0.01 μ M), but not altered by puerarin (100 μ M–1000 μ M) (Fig. 5A and B). Furthermore, the fluorescence based In Situ TUNEL staining assay indicated that the osteoclast apoptosis rate was significantly increased by E_2 (0.01 μ M). However, puerarin slightly decreased osteoclast apoptosis without significant differences (Fig. 5C and D).

3.5. Puerarin prevented rats from OVX-induced bone loss and improved femoral mechanical properties

Micro CT analysis was carried out to examine the bone mass and structures of proximal tibia. In the long-term study of 12 weeks, as to trabecular bone at proximal tibia, decreased BMD, BV/TV, Conn. D, Tb. N, Tb. Sp, and Tb. Th were observed in OVX group, compared to those in Sham group. Compared to OVX group, puerarin prevented bone loss in a dose dependent manner. L-Puerarin group had no effect on trabecular bone at proximal tibia, while H-Puerarin group showed significantly higher BMD, BV/TV, Conn. D, Tb. N, Tb. Th and lower Tb. Sp (Fig. 6A and B). Thus, we chose the high dose of puerarin in the following short-term (treatment for 5 weeks) efficacy and mechanism study, and similar results were obtained (Fig. 6A and B). Further observations by Von Kossa staining analysis of proximal tibia metaphysis administrated for 5 weeks provided additional supports for that H-Puerarin had higher BV/TV, Tb. Wi, Tb. N and lower Tb. Sp compared to those in OVX group (Fig. 6C and D).

Three-point bending was used to test the mechanical property of the cortical bone at femur shaft. Ultimate load and energy to failure of femur

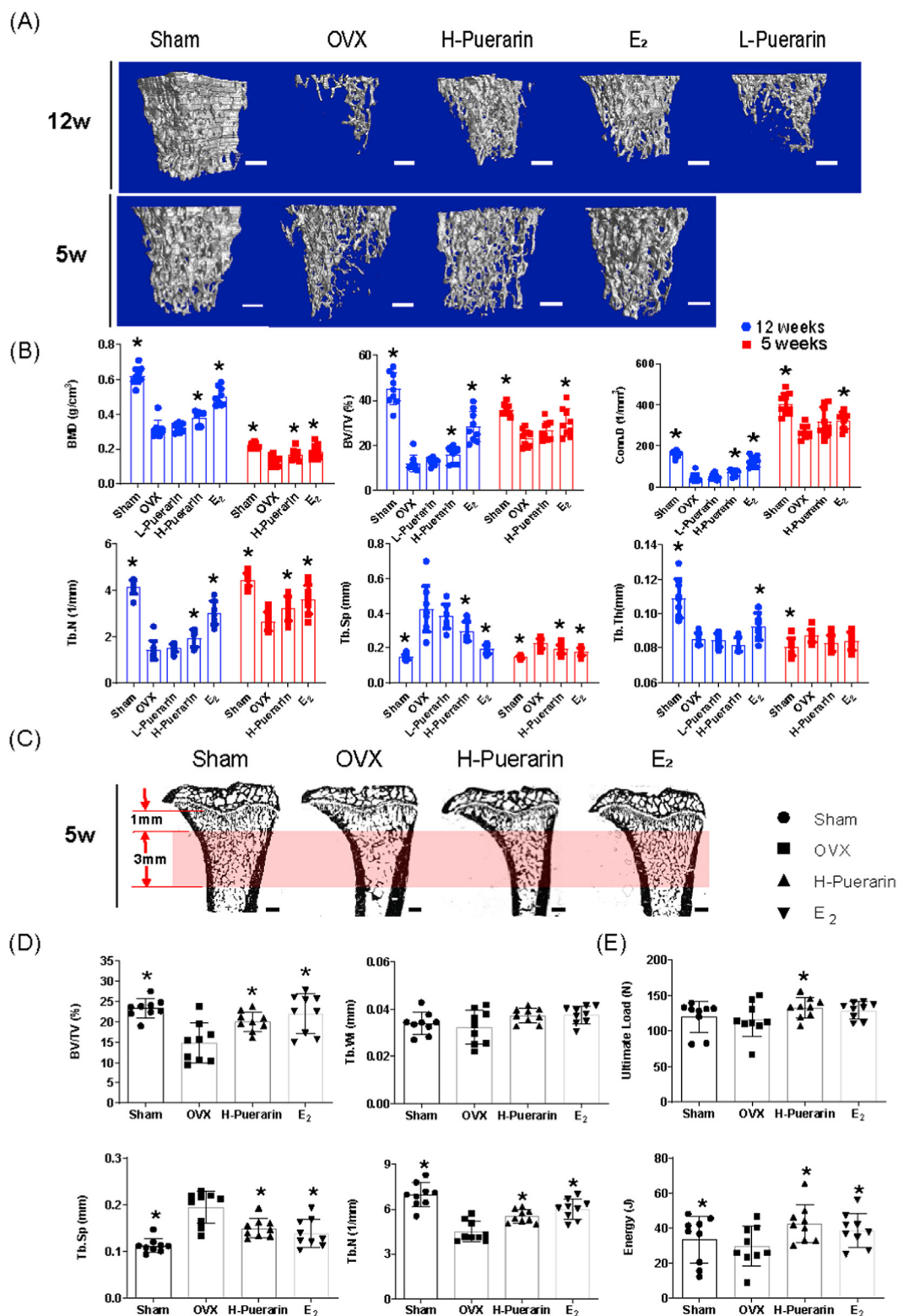


Figure 6. High dose of puerarin decreases OVX-induced bone loss and improves mechanical properties (A) Representative 3D reconstruction images of proximal tibia metaphysis for 12 weeks and 5 weeks. Scale bar: 1 mm (B) Quantitative analysis of micro-CT parameters of trabecular bone including BMD, BV/TV, Conn. D, Tb. N, Tb. Sp and Tb. Th for 12 weeks (n = 9) and 5 weeks (n = 9) (C) Representative image of undecalcified proximal tibia metaphysis stained with Von Kossa staining from each group. Black Scale bar: 500 μ m (D) Quantitative analysis of Static histological parameters including BV/TV, Tb. Wi, Tb. Sp and Tb. N (n = 9). ROI of micro CT and histomorphometric analysis were defined from 1 mm to 4 mm below growth plate (E) Left femurs were isolated and subjected to a three-point bending tests. The ultimate load and energy to failure were evaluated (n = 9). BMD: Bone mineral density; BV/TV: Bone volume fraction; Conn. Dn: Connectivity density; Tb. N: Trabecular number; Tb. Sp: Trabecular separation; Tb. Th: Trabecular thickness; Tb. Wi: Trabecular width. Data expressed are means \pm SD; *P < 0.05 compared to OVX group.

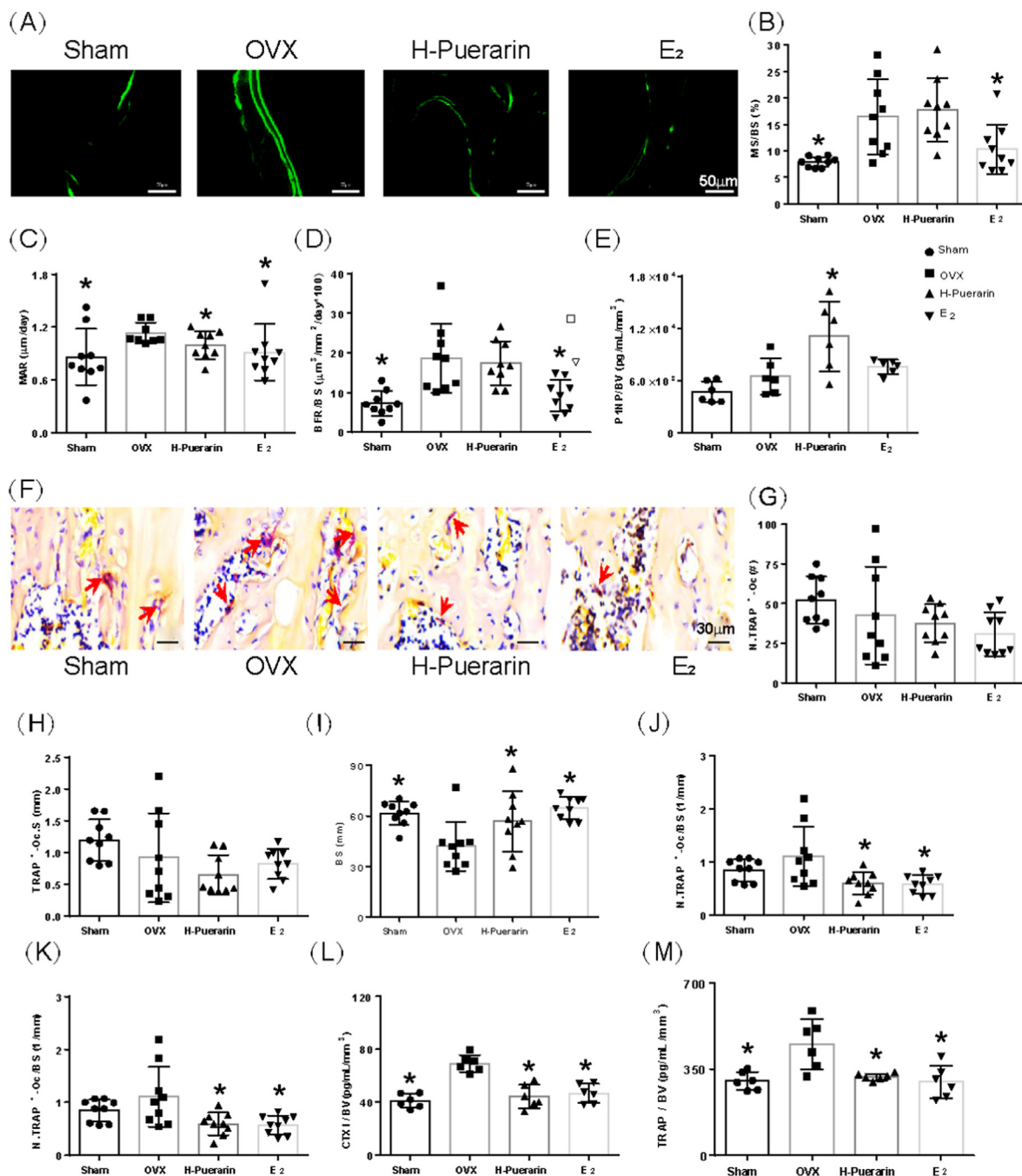


Fig. 7. Puerarin inhibits bone resorption to prevent bone loss (A) Representative images of trabecular fluorescence labeling of proximal tibia metaphysis. Scale bar: 50 μm . Quantitative analysis of (B) MS/BS (n = 9) (C) MAR (n = 9) and (D) BFR/BS (n = 9). Biomarker of bone formation such as (E) PINP normalized by bone volume in serum (n = 6) (F) Representative TRAP staining micrograph and (G–K) quantitative data of N. TRAP⁺ Oc, TRAP⁺ Oc.S, BS, N.TRAP⁺ Oc/BS and TRAP⁺ Oc.S/BS. Red arrow pointed to TRAP positive osteoclast (n = 6) for each group to evaluate indicators of the osteoclast (L–M) CTX1 (n = 6) and Trap (n = 6) normalized by bone volume in serum. MS/BS: Mineralizing surface; MAR: Mineral apposition rate; BFR/BS: Bone formation rate; N.TRAP⁺ Oc: Number of TRAP positive osteoclast; TRAP⁺ Oc.S: TRAP positive osteoclast surface; BS: Bone surface; N.TRAP⁺ Oc/BS: Number fraction of TRAP positive osteoclast normalized by bone surface; TRAP⁺ Oc.S/BS: TRAP positive osteoclast surface fraction normalized by bone surface. Data expressed are means \pm SD; *P < 0.05 compared to OVX group.

diaphysis between Sham group and OVX group were similar. Compared to OVX group, H-Puerarin group had 13.69% higher ultimate load and 43.22% higher energy, while E₂ group had 31.49% higher energy compared to OVX group (Fig. 6E).

3.6. Puerarin significantly prevented OVX-induced bone loss by inhibiting bone resorption but not altering bone formation

Dynamic histomorphometry and serum biomarkers were used to

investigate how puerarin regulated bone metabolism. Representative double fluorescence on trabecular bone at the proximal tibial metaphysis was shown in Fig. 7A. Quantitative results showed that E₂ group had significantly less MS/BS, MAR and BFR/BS compared with those in the OVX group (37.20%, 28.94% and 50.28%, respectively). H-puerarin group had no effect on MS/BS and BFR/BS compared with that in OVX group (Fig. 7B–D). Serum PINP normalized by bone volume in H-Puerarin group was 70.58% more than that in OVX group (Fig. 7E). Fig. 7F showed representative TRAP staining osteoclasts at the proximal tibial

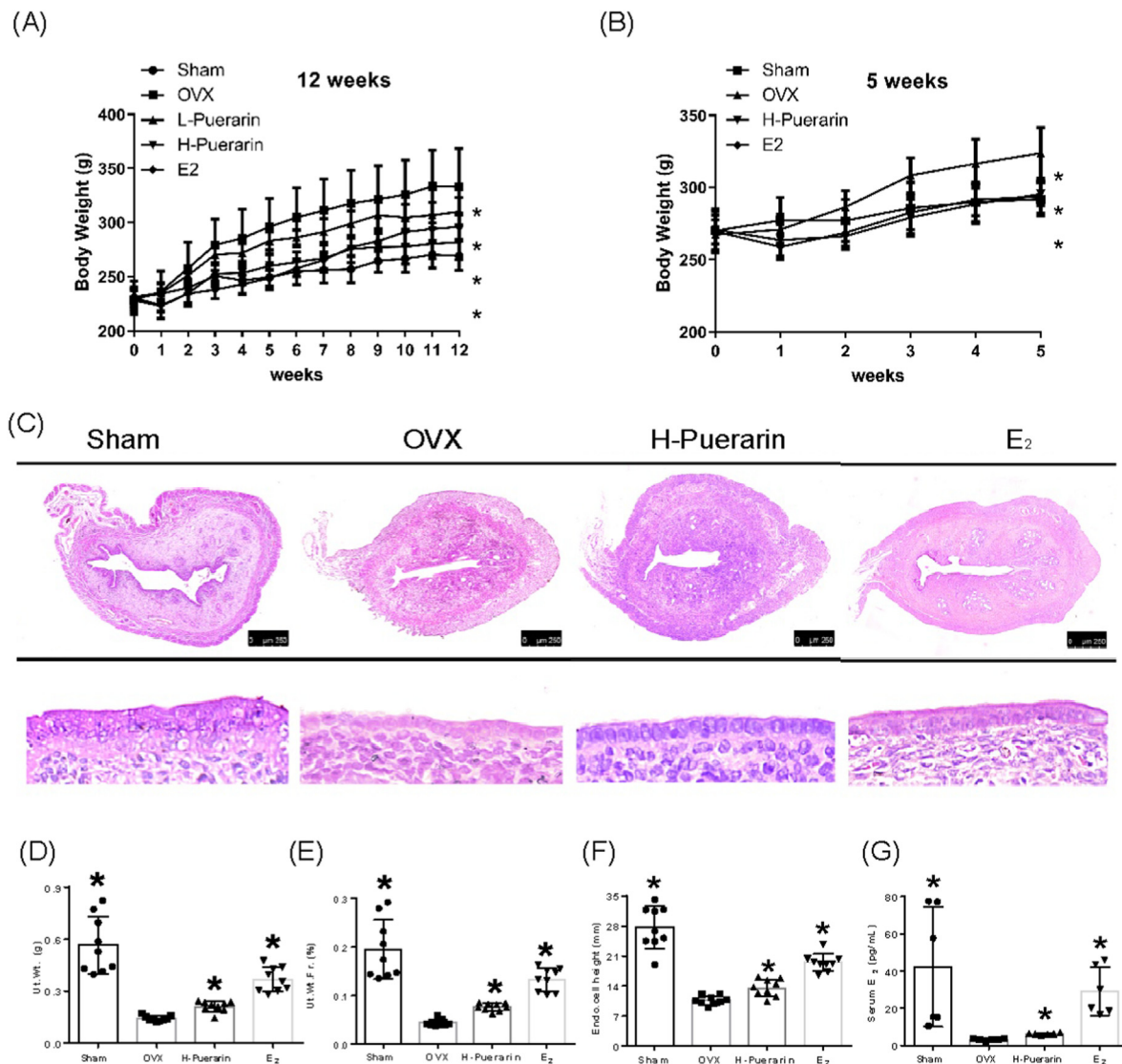


Fig. 8. Puerarin inhibits OVX induced body weight increase and has a weaker hypertrophic effect on uterus. Body weight were recorded every week in long term study (A, 12 weeks, n = 9 for each group) and short-term study (B, 5 weeks, n = 9 for each group) (C) Representative histologic micrograph of uterine cross section and endothelial cell thickness (D–F) Quantitative data of uterine weight (n = 9 for each group), uterine weight fraction (n = 9 for each group) and endometrial cell height (n = 9 for each group). (G) Concentration of estradiol in serum (n = 6 for each group). Ut. Wt.: Uterine Weight; Ut.Wt.Fr.: Uterine Weight Fraction; Endo. cell height: Endometrial cell height. Data expressed are means ± SD; *P < 0.05 compared to OVX group.

metaphysis. H-Puerarin and E₂ had lower N.TRAP⁺-Oc/BS and TRAP⁺-Oc.S/BS (Fig. 7 G-K). In addition, serum CTx1 (Fig. 7L) and Trap (Fig. 7M), which were both normalized by bone volume in H-Puerarin and E₂ group, were less than those in OVX group.

3.7. Effect of puerarin on body weight, uterine weight and uterine histomorphometry

Both H-Puerarin and E₂ group significantly inhibited the increase of body weight induced by OVX surgery from 2 weeks to 12 weeks (Fig. 8A) or 5 weeks post-surgery (Fig. 8B). Histologically, E₂ group significantly increased the endometrial cell height relative to OVX group, while puerarin slightly increased it (Fig. 8C). Compared to OVX, H-Puerarin increased uterus weight by 1.58 folds, but lower than estrogen which increased by 3 folds (Fig. 8D and E). E₂ and H-Puerarin had 77.77% and 26.18% higher endometrial cell height than OVX (Fig. 8F), respectively. After surgery for 5 weeks, serum estradiol concentration decreased from 42.29 pg/mL in Sham group to 3.17 pg/mL in OVX group, while exogenous estrogen administration increased serum

estrogen concentration to 29.22 pg/mL, and H-Puerarin increased it to 6.15 pg/mL (Fig. 8G).

4. Discussion

In the present study we demonstrated that puerarin, a C-glycoside isoflavonoid, prevents the bone loss in OVX rat through suppression of osteoclast activation and bone resorption without suppressing bone formation. For the first time it is revealed that puerarin inhibits osteoclasts activation by disrupting F-actin ring formation via integrin β3/Pyk2/Src/Cbl signaling pathway, without affecting osteoclastogenesis or apoptosis.

Bone resorption is a well-controlled process, including osteoclastogenesis to form polykaryon, activation of osteoclasts by forming F-actin rings and sealed zone, and then resorption by secretion of acids and lysosomal enzymes onto the resorbing surface [33]. Firstly, several lines evidence have demonstrated that puerarin didn't directly inhibit bone resorption, because bone resorption still occurred when puerarin was added to the medium at day 5–7 after RANKL induction. Also, the osteoclastic bone resorption related genes including MMP9 and CTSK [34],

had not changed at all even the cells were treated by puerarin during the whole process. From this respect, puerarin is different from natural dihydroflavone and dihydrotanshinone I, which inhibits the expression or activity of cathepsin K leading to suppressing bone resorption [24,35].

Secondly, puerarin didn't affect the early stage of osteoclastogenesis (cell fusion) but impaired F-actin ring formation during osteoclast activation. This conclusion was supported by the data that number and size of MNCs in puerarin group were similar with the un-treatment group. Instead, the fluorescence intensity and protein expression of integrin- β 3 (major protein responsible for F-actin mediated osteoclast attachment) was attenuated by puerarin. RANK-specific activation of TRAF6 leads to induction of NFATc1, which is critical for osteoclastogenesis [36]. When the cells are activated by RANKL, NFATc1 expression is dependent on the TRAF6/NF- κ B and c-Fos pathways [37]. Our data showed that puerarin significantly down regulated c-Fos gene expression, while did not suppress the expression of NF- κ B and phospho-NF- κ B, and the overall outcome was that gene and protein expressions of NFATc1 were not inhibited by puerarin, which was consistent with a previous study [21]. However, two recently published articles from the same group reported a different finding, which indicated that puerarin (100 μ M) suppressed osteoclastogenesis via inhibition of NF- κ B signaling pathways in both osteoclast of RANKL-induced BMMs and RAW264.7 cells [17,18]. Although they reported that F-actin ring formation and bone resorption were also decreased by puerarin, the authors consider these as the cascade events following the suppression of osteoclastogenesis. Our data showed that puerarin disturbed the F-actin ring formation rather than inhibited their differentiation from osteoclast precursors. Further compelling evidence for this conclusion was given by the expression of OC-STAMP, a putative seven-transmembrane spanning protein, is essential for early events in osteoclastogenesis, *i.e.*, the cell-cell fusion of osteoclast precursors [38]. We found that puerarin didn't affect mRNA expression of OC-STAMP or cell-cell fusion. In addition, SEM images clearly showed us osteoclasts in puerarin group were formed in the bone slice but lack of marginal wrinkle compared to the untreated ones.

Thirdly, we firstly found that puerarin had no effect on osteoclasts apoptosis as it didn't alter the ratio of cleaved caspase-3/caspase-3 or TUNEL positive cells, while estradiol promoted apoptosis as previously reported [39]. The survival of the mature osteoclast, and its participation in successive rounds of bone resorption, is regulated in part by inducing NF- κ B activity [40]. We found that the expression of phosphorylated NF- κ B (p65) was not down-regulated by puerarin, which suggested puerarin didn't influence osteoclasts survival either. Thus, puerarin does not affect fused polykaryon formation, degradation of bone matrix and osteoclasts apoptosis.

Actin ring is a characteristic of active osteoclasts [33]. It is a unique cytoskeletal structure for the formation of a sealing zone responsible for osteoclast attachment, and subsequently bone resorption [41]. Integrin β 3 was the major adhesion receptor required for the formation of the sealing zone. Osteoclasts isolated from integrin β 3-deficient mice failed to spread, lacked actin rings characteristic of active osteoclasts and exhibited reduced bone resorption activity *in vitro*, indicating the critical role of integrin- β 3 in osteoclast attachment [33]. In order to further clarify the precise mechanism of puerarin on disruption F-actin ring formation, integrin- β 3 mediated Pyk2/Src/Cbl pathway was investigated. Our present results clearly indicated that activated protein expression of integrin- β 3 mediated Pyk2/Src/Cbl signaling molecules induced by RANKL were greatly abrogated by puerarin. The adapter function and kinase activity of Src were both required for the formation of Pyk2/Src/Cbl complex and osteoclast function [42]. Our results demonstrated that puerarin had no effect on inhibiting Src kinase activity, which indicated that puerarin was not a direct Src kinase inhibitor. Our results indicated that the immunofluorescence of integrin β 3 was significantly attenuated by the treatment of puerarin, which suggest puerarin may affect cell attachment of osteoclast via impairing integrin- β 3 binding to extracellular matrix proteins. Downstream of integrin- β 3/Pyk2/Src/Cbl signaling pathway, other cytoskeletal adaptors that

organize F-actin were also determined, paxillin is an adhesion plaque protein that organized F-actin, and gelsolin is a high-affinity actin-severing protein that promotes actin turnover, they are important structural proteins that organized F-actin [43]. Our results indicated that gelsolin, but not paxillin, was suppressed by 1000 μ M of puerarin. NFATc1 forms an osteoclast-specific transcriptional complex containing AP-1 (Fos/Jun) for the efficient induction of osteoclast-specific genes, such as integrin- β 3 [44,45]. Puerarin significantly blocked c-Fos expression, which might contribute to abrogation of gene and protein expression of integrin- β 3. Thus, integrin- β 3 mediated Pyk2/Src/Cbl pathway was impaired by puerarin, resulting in disruption F-actin ring formation and successive inactivation of osteoclasts. We speculated that the direct target of puerarin is most likely to be the protein located in the upstream of integrin- β 3 mediated Pyk2/Src/Cbl signaling pathway, our future work will focus on the target discovery of puerarin.

In vivo, most of previous study of puerarin perform the long-term (12 weeks) administration, which is common treatment duration for traditional Chinese Medicine in osteoporosis study [46]. So, we investigated dose-dependent effect of puerarin in this long-term experiment. Short-term is a 5-week treatment after OVX surgery, when bone resorption is active and the significant bone loss in proximal tibia metaphysis occurred in OVX rats [47]. Thus, this time point is great for both efficacy and *in vivo* mechanistic study, especially for bone resorption matching *in vitro* [48]. In the term study, we confirmed the efficacy of high dose puerarin on preventing bone loss. In addition, we investigated the *in vivo* anti-resorption mechanism of puerarin by using trap staining and serum biomarkers evaluations.

Dynamic histomorphometry and serum biomarker analysis revealed us unique feature of puerarin on preventing bone loss. Lower TRAP⁺ Oc.N/BS, serum TRAP 5b, CTx1 and unchanged BFR/BS in H-puerarin group in relative to OVX group consistently revealed puerarin inhibited bone resorption without affecting bone formation *in vivo*. This was obviously different with E₂, as it not only decreased Oc.N/BS, serum TRAP 5b and CTx1, but also inhibited BFR/BS, which indicated a decrease in bone formation due to disrupting the osteoclast-osteoblast crosstalk [49]. This is an advantage of puerarin over estradiol, which is achieved by the fact that puerarin didn't influence osteoclastogenesis and apoptosis. From osteoclast-osteoblast coupling aspect, puerarin has an advantage over estradiol by avoidance of interfering with osteoclast-related bone formation because it allows the crosstalk between osteoclasts and osteoblasts to remain intact, which is beneficial for the ongoing bone formation.

Isoflavone was commonly considered as phytoestrogen due to their biphenolic structure. In order to evaluate if puerarin exerted similar effect and mechanism as estrogen, 17- β estradiol was used as positive control in our present study. We found that puerarin slightly promote uterus hypertrophy, similar results demonstrated that puerarin possessed property of partial agonist of ER [50]. Puerarin was proved not to bind into estrogen receptor (ER) [51], and exerted bone loss-preventing action independently of ER-mediated pathway [51]. It can be explained by our data that puerarin promoted endogenous estradiol production, from 3.22 pg/mL in OVX group to 6.4 pg/mL in H-puerarin, which is discovered for the first time by using UPLC-MS, a more specific and sensitive testing methods than ELISA [53]. The mechanism of puerarin promoting endogenous estradiol production in OVX rats needs to be studied further.

5. Conclusions

In summary, puerarin specifically suppressed activation of osteoclasts through disruption of F-actin ring formation by abrogating integrin- β 3/Pyk2/Src/Cbl pathway and inhibited bone resorption *in vitro* and *in vivo*. These findings provide a natural C-glycoside isoflavonoid structure targeting suppression of osteoclast activation without interfering with the crosstalk between osteoclasts and osteoblasts, which may overcome the shortcomings of bone formation-suppression of anti-resorption drugs, such as estradiol and bisphosphonate.

Funding

This work was supported by the National Natural Science Foundation of China (81773964, 81903618), Guangdong Basic and Applied Basic Research Foundation (2021B1515120061), Guangzhou Basic and Applied Basic Research Foundation (202102021160), Shenzhen International Collaborative Project (GJHZ20190821160803823), Guangdong Provincial Key Laboratory of Traditional Chinese Medicine Informatization (2021B1212040007).

Author contributions

Study design: XLW and QQZ. Study conduct: LL and ZCQ. Data collection: YYH, JLW, ZCQ, LL. Data analysis: CSH, KDS, LLZ, JCL, ZCQ and LL. Data interpretation: ZCQ, LL, QQZ and XLW. Drafting manuscript: ZCQ, LL and XLW. Revising manuscript content: XJH, LQ and XLW. Approving final version of manuscript: LQ and XLW. XLW takes responsibility for the integrity of the data analysis.

Authorship

All persons who meet authorship criteria are listed as authors, and all authors certify that they have participated sufficiently in the work to take public responsibility for the content, including participation in the concept, design, analysis, writing, or revision of the manuscript. Each author certifies that this material or part thereof has not been published in another journal, that it is not currently submitted elsewhere, and that it will not be submitted elsewhere until a final decision regarding publication of the manuscript in *Journal of Orthopaedic Translation* has been made. Indicate the specific contributions made by each author (list the authors' initials followed by their surnames, e.g., Y.L. Cheung). The name of each author must appear at least once in each of the three categories below.

Declaration of competing interest

A conflict of interest occurs when an individual's objectivity is potentially compromised by a desire for financial gain, prominence, professional advancement or a successful outcome. The Editors of the *Journal of Orthopaedic Translation* strive to ensure that what is published in the Journal is as balanced, objective and evidence-based as possible. Since it can be difficult to distinguish between an actual conflict of interest and a perceived conflict of interest, the Journal requires authors to disclose all and any potential conflicts of interest.

Appendix A. Supplementary data

Supplementary data to this article can be found online at <https://doi.org/10.1016/j.jot.2022.01.003>.

References

- Rachner TD, Khosla S, Hofbauer LC. Osteoporosis: now and the future. *Lancet* 2011; 377(9773):1276–87.
- Zheng N, Tang N, Qin L. Atypical femoral fractures and current management. *J Orthop Translat* 2016;7:7–22.
- Takahashi N, Ejiri S, Yanagisawa S, Ozawa H. Regulation of osteoclast polarization. *Odontology* 2007;95(1):1–9.
- Panwar P, Law S, Jamroz A, Azizi P, Zhang D, Ciufolini M, et al. Tanshinones that selectively block the collagenase activity of cathepsin K provide a novel class of ectosteric antiresorptive agents for bone. *Br J Pharmacol* 2018;175(6):902–23.
- Kameda T, Mano H, Yuasa T, Mori Y, Miyazawa K, Shiokawa M, et al. Estrogen inhibits bone resorption by directly inducing apoptosis of the bone-resorbing osteoclasts. *J Exp Med* 1997;186(4):489–95.
- Wang Y, Wang WL, Xie WL, Li LZ, Sun J, Sun WJ, et al. Puerarin stimulates proliferation and differentiation and protects against cell death in human osteoblastic MG-63 cells via ER-dependent MEK/ERK and PI3K/Akt activation. *Phytomedicine* 2013;20(10):787–96.
- Panwar P, Xue L, Soe K, Srivastava K, Law S, Delaisse JM, et al. An ectosteric inhibitor of cathepsin K inhibits bone resorption in ovariectomized mice. *J Bone Miner Res* 2017;32(12):2415–30.
- Zhu HM, Qin L, Garnerio P, Genant HK, Zhang G, Dai K, et al. The first multicenter and randomized clinical trial of herbal Fufang for treatment of postmenopausal osteoporosis. *Osteoporos Int* 2012;23(4):1317–27 [eng].
- Chen SH, Wang XL, Zheng LZ, Dai Y, Zhang JY, Guo BL, et al. Comparative study of two types of herbal capsules with different *Epimedium* species for the prevention of ovariectomized-induced osteoporosis in rats. *Journal of Orthopaedic Translation* 2016;4(1):14–27.
- Chen SH, Wang XL, Zheng LZ, Dai Y, Zhang JY, Guo BL, et al. Comparative study of two types of herbal capsules with different *Epimedium* species for the prevention of ovariectomized-induced osteoporosis in rats. *J Orthop Translat* 2016;4:14–27.
- Tanaka T, Tang H, Yu F, Michihara S, Uzawa Y, Zaima N, et al. Kudzu (*Pueraria lobata*) vine ethanol extracts improve ovariectomy-induced bone loss in female mice. *J Agric Food Chem* 2011;59(24):13230–7.
- Zhou YX, Zhang H, Peng C. Puerarin: a review of pharmacological effects. *Phytother Res* 2014;28(7):961–75.
- Wang Q, Wu T, Chen X, Ni J, Duan X, Zheng J, et al. Puerarin injection for unstable angina pectoris. *Cochrane Database Syst Rev* 2006;3:CD004196.
- Tan Y, Liu M, Wu B. Puerarin for acute ischaemic stroke. *Cochrane Database Syst Rev* 2008;1:CD004955.
- Wang N, Wang X, Cheng W, Cao H, Zhang P, Qin L. Puerarin promotes osteogenesis and inhibits adipogenesis in vitro. *Chin Med* 2013;8(1):17.
- Yuan SY, Sheng T, Liu LQ, Zhang YL, Liu XM, Ma T, et al. Puerarin prevents bone loss in ovariectomized mice and inhibits osteoclast formation in vitro. *Chin J Nat Med* 2016;14(4):265–9.
- Tang W, Xiao L, Ge G, Zhong M, Zhu J, Qin J, et al. Puerarin inhibits titanium particle-induced osteolysis and RANKL-induced osteoclastogenesis via suppression of the NF-kappaB signaling pathway. *J Cell Mol Med* 2020;24(20):11972–83.
- Xiao L, Zhong MD, Huang Y, Zhu J, Tang WK, Li DY, et al. Puerarin alleviates osteoporosis in the ovariectomy-induced mice by suppressing osteoclastogenesis via inhibition of TRAF6/ROS-dependent MAPK/NF-kB signaling pathways. *Aging* 2020; 12(21):21706–29.
- Li B, Liu H, Jia S. Puerarin enhances bone mass by promoting osteoblastogenesis and slightly lowering bone marrow adiposity in ovariectomized rats. *Biol Pharm Bull* 2014;37(12):1919–25.
- Zhang Y, Yan M, Yu QF, Yang PF, Zhang HD, Sun YH, et al. Puerarin prevents LPS-induced osteoclast formation and bone loss via inhibition of Akt activation. *Biol Pharm Bull* 2016;39:2028–35.
- Park KH, Gu DR, Jin SH, Yoon CS, Ko W, Kim YC, et al. *Pueraria lobata* inhibits RANKL-mediated osteoclastogenesis via downregulation of CREB/PGC1beta/c-Fos/NFATc1 signaling. *Am J Chin Med* 2017;45(8):1725–44.
- Guo W, Li H, Lou Y, Zhang Y, Wang J, Qian M, et al. Tyloxapol inhibits RANKL-stimulated osteoclastogenesis and ovariectomized-induced bone loss by restraining NF-kappaB and MAPK activation. *J Orthop Translat* 2021;28:148–58.
- Qiu ZC, Tang XY, Wu QC, Tang ZL, Wong MS, Chen JX, et al. A new strategy for discovering effective substances and mechanisms of traditional Chinese medicine based on standardized drug containing plasma and the absorbed ingredients composition, a case study of Xian-Ling-Gu-Bao capsules. *J Ethnopharmacol* 2021; 279:114396.
- Qiu ZC, Dong XL, Dai Y, Xiao GK, Wang XL, Wong KC, et al. Discovery of a new class of cathepsin K inhibitors in rhizoma *drynariae* as potential candidates for the treatment of osteoporosis. *Int J Mol Sci* 2016;17(12).
- Zhou CH, Shi ZL, Meng JH, Hu B, Zhao CC, Yang YT, et al. Sophocarpine attenuates wear particle-induced implant loosening by inhibiting osteoclastogenesis and bone resorption via suppression of the NF-kappaB signalling pathway in a rat model. *Br J Pharmacol* 2018;175(6):859–76.
- Dempster DW, Compston JE, Drezner MK, Glorieux FH, Kanis JA, Malluche H, et al. Standardized nomenclature, symbols, and units for bone histomorphometry: a 2012 update of the report of the ASBMR Histomorphometry Nomenclature Committee. *J Bone Miner Res* 2013;28(1):2–17.
- Bouxsein ML, Boyd SK, Christiansen BA, Guldberg RE, Jepsen KJ, Muller R. Guidelines for assessment of bone microstructure in rodents using micro-computed tomography. *J Bone Miner Res* 2010;25(7):1468–86.
- Li L, Yi X, Huang C, Shi K, Wang J, Zeng Q, et al. Qu Feng Zhi Tong capsule increases mechanical properties of cortical bone in ovariectomized rats. *Journal of Orthopaedic Translation* 2020;25:115–24.
- Xiao HH, Dai Y, Wan HY, Wong MS, Yao XS. Bone-protective effects of bioactive fractions and ingredients in *Sambucus williamsii* HANCE. *Br J Nutr* 2011;106(12): 1802–9.
- Rissanen JP, Suominen MI, Peng Z, Morko J, Rasi S, Risteli J, et al. Short-term changes in serum PINP predict long-term changes in trabecular bone in the rat ovariectomy model. *Calcif Tissue Int* 2008;82(2):155–61 [eng].
- Kushnir MM, Rockwood AL, Bergquist J, Varshavsky M, Roberts WL, Yue B, et al. High-sensitivity tandem mass spectrometry assay for serum estrone and estradiol. *Am J Clin Pathol* 2008;129(4):530–9.
- Tang XY, Dai ZQ, Shi DF, Zeng JX, Wang XL, Li L, et al. An UHPLC-MS/MS method for simultaneous determination of ten sex steroid hormones in ovariectomy-induced osteoporosis rat and its application in discovery of sex steroid hormones regulatory components of Xian-Ling-Gu-Bao capsule. *J Pharmaceut Biomed* 2021:195 [English].
- Nakamura I, Duong LT, Rodan SB, Rodan GA. Involvement of alpha(v)beta3 integrins in osteoclast function. *J Bone Miner Metabol* 2007;25(6):337–44.
- Cappariello A, Maurizi A, Veeriah V, Teti A. The great beauty of the osteoclast. *Arch Biochem Biophys* 2014;558:70–8.

- [35] Panwar P, Soe K, Guido RV, Bueno RV, Delaisse JM, Bromme D. A novel approach to inhibit bone resorption: exosite inhibitors against cathepsin K. *Br J Pharmacol* 2016;173(2):396–410.
- [36] Gohda J, Akiyama T, Koga T, Takayanagi H, Tanaka S, Inoue J. RANK-mediated amplification of TRAF6 signaling leads to NFATc1 induction during osteoclastogenesis. *EMBO J* 2005;24(4):790–9.
- [37] Takayanagi H. The role of NFAT in osteoclast formation. *Ann N Y Acad Sci* 2007;1116(1):227–37.
- [38] Witwicka H, Hwang SY, Reyes-Gutierrez P, Jia H, Odgren PE, Donahue LR, et al. Studies of OC-STAMP in osteoclast fusion: a new knockout mouse model, rescue of cell fusion, and transmembrane topology. *PLoS One* 2015;10(6):e0128275.
- [39] Boyce BF. Advances in the regulation of osteoclasts and osteoclast functions. *J Dent Res* 2013;92(10):860–7.
- [40] Ono T, Nakashima T. Recent advances in osteoclast biology. *Histochem Cell Biol* 2018;149(4):325–41.
- [41] Takito J, Otsuka H, Yanagisawa N, Arai H, Shiga M, Inoue M, et al. Regulation of osteoclast multinucleation by the actin cytoskeleton signaling network. *J Cell Physiol* 2015;230(2):395–405.
- [42] Miyazaki T, Sanjay A, Neff L, Tanaka S, Horne WC, Baron R. Src kinase activity is essential for osteoclast function. *J Biol Chem* 2004;279(17):17660–6.
- [43] Georgess D, Machuca-Gayet I, Blangy A, Jurdic P. Podosome organization drives osteoclast-mediated bone resorption. *Cell Adhes Migrat* 2014;8(3):191–204.
- [44] Crotti TN, Flannery M, Walsh NC, Fleming JD, Goldring SR, McHugh KP. NFATc1 directly induces the human beta3 integrin gene in osteoclast differentiation. *J Musculoskelet Neuronal Interact* 2005;5(4):335–7.
- [45] Crotti TN, Sharma SM, Fleming JD, Flannery MR, Ostrowski MC, Goldring SR, et al. Pu.1 and NFATc1 mediate osteoclastic induction of the mouse beta3 integrin promoter. *J Cell Physiol* 2008;215(3):636–44.
- [46] Li BB, Liu H, Jia SN. Puerarin enhances bone mass by promoting osteoblastogenesis and slightly lowering bone marrow adiposity in ovariectomized rats. *Biol Pharm Bull* 2014;37(12):1919–25 [English].
- [47] Kakehashi A, Yoshida M, Tago Y, Ishii N, Okuno T, Gi M, et al. Pueraria mirifica exerts estrogenic effects in the mammary gland and uterus and promotes mammary carcinogenesis in donryu rats. *Toxins* 2016;8(11).
- [48] Wronski TJ, Cintron M, Dann LM. Temporal relationship between bone loss and increased bone turnover in ovariectomized rats. *Calcif Tissue Int* 1988;43(3):179–83 [English].
- [49] Liu L, Zhou L, Yang X, Liu Q, Yang L, Zheng C, et al. 17beta-estradiol attenuates ovariectomy-induced bone deterioration through the suppression of the ephA2/ephrinA2 signaling pathway. *Mol Med Rep* 2018;17(1):1609–16.
- [50] Zheng G, Zhang X, Zheng J, Meng Q, Zheng D. [Estrogen-like effects of puerarin and total isoflavones from *Pueraria lobata*]. *Zhong Yao Cai* 2002;25(8):566–8.
- [51] Michihara S, Tanaka T, Uzawa Y, Moriyama T, Kawamura Y. Puerarin exerted anti-osteoporotic action independent of estrogen receptor-mediated pathway. *J Nutr Sci Vitaminol* 2012;58(3):202–9.
- [52] Faupel-Badger JM, Fuhrman BJ, Xu X, Falk RT, Keefer LK, Veenstra TD, et al. Comparison of liquid chromatography-tandem mass spectrometry, RIA, and ELISA methods for measurement of urinary estrogens. *Cancer Epidemiol Biomarkers Prev* 2010;19(1):292–300.